Article

Structural and Electron-Transfer Characteristics of O-, S-, and Se-Tethered Porphyrin Monolayers on Si(100)

Amir A. Yasseri, Dennis Syomin, Robert S. Loewe,
Jonathan S. Lindsey, Francisco Zaera, and David F. Bocian

J. Am. Chem. Soc., **2004**, 126 (47), 15603-15612• DOI: 10.1021/ja045243w • Publication Date (Web): 09 November 2004

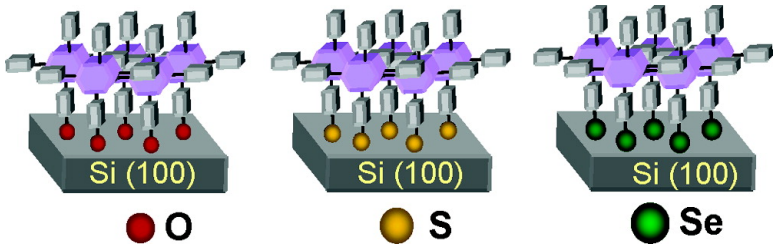

More About This Article

Additional resources and features associated with this article are available within the HTML version:

- Supporting Information
- Links to the 10 articles that cite this article, as of the time of this article download
- Access to high resolution figures
- Links to articles and content related to this article
- Copyright permission to reproduce figures and/or text from this article

View the Full Text HTML

J|A|C|S
ARTICLES
Published on Web 11/09/2004

Structural and Electron-Transfer Characteristics of O-, S-, and Se-Tethered Porphyrin Monolayers on Si(100)

Amir A. Yasseri,[†] Dennis Syomin,[†] Robert S. Loewe,[‡] Jonathan S. Lindsey,*[,‡] Francisco Zaera,*[,†] and David F. Bocian*[,†]

Contribution from the Department of Chemistry, University of California, Riverside, California 92521-0403 and Department of Chemistry, North Carolina State University, Raleigh, North Carolina 27695-8204

Received August 6, 2004; E-mail: jlindsey@ncsu.edu; Francisco.Zaera@ucr.edu; David.Bocian@ucr.edu

Abstract: Monolayers of two classes of Zn porphyrins have been prepared and examined on Si(100). These molecules, designated as **ZnPBzX**− and **ZnPCH$_2$X**−, contain either a benzyl (−**Bz**−**)** or a methylene (−**CH$_2$**−) unit terminated with a Group VI atom (X = O, S, Se) appended to a *meso*-position of the porphyrin, with the nonlinking meso-substituents consisting of either mesityl (−**Bz**− class) or *p*-tolyl and phenyl (−**CH$_2$**− class) units. The two series of **ZnPBzX**− and **ZnPCH$_2$X**− monolayers on Si(100) were examined using a variety of techniques, including X-ray photoelectron spectroscopy, Fourier transform infrared spectroscopy, and various electrochemical methods. The studies reveal the following characteristics of the **ZnPBzX**− and **ZnPCH$_2$X**− monolayers. (1) Surface binding can be readily achieved to Si(100) with both relatively short (−**Bz**−) and very short (−**CH$_2$**−) tethers regardless of the nature of the Group VI anchoring atom (O, S, Se). (2) The longer −**Bz**− tether affords monolayers with the porphyrin ring in a somewhat more upright orientation with respect to the surface than the shorter −**CH$_2$**− tether. The more upright adsorption geometry of the porphyrins bearing the former type of linker leads to a higher packing density and more homogeneous redox thermodynamics. (3) The kinetics of electron transfer does not depend on the type of Group VI atom used for anchoring to the Si(100) surface. On the other hand, the type of linker does affect the electron-transfer rates, with the monolayers bearing the −**CH$_2$**− linker exhibiting systematically faster rates than those bearing the −**Bz**− linker. Collectively, the studies reported herein provide a detailed picture of how the anchor atom and the linker type influence the structural and electron-transfer characteristics of these general classes of monolayers.

I. Introduction

The field of molecular electronics is driven by the prospect that devices relying on the bulk properties of semiconductors will fail to retain their characteristic properties as sizes reach nanoscale dimensions.[1] Nevertheless, early generations of electronic devices based on molecular materials will most likely be some type of hybrid molecular/semiconductor design. Indeed, efforts are underway to develop hybrid platforms for both memory and logic applications.[2−4] Our group has focused on memory applications wherein molecules attached to an electroactive surface serve as the active medium. In this approach, information is stored in discrete molecules by taking advantage of their multiple stable oxidation states. The ability to store charge in the surface-bound molecules allows the molecular medium to mimic the function of semiconductor capacitors, such as those found in dynamic random access memory cells.[5]

In our hybrid molecular/semiconductor architectures, the electroactive molecules include porphyrin or ferrocene species covalently linked to a semiconductor (or oxide) surface via a tether bearing a terminal functional group. We have principally used alcohols (and to a lesser extent phosphonates) for linking the electroactive molecules to Si and SiO_2 surfaces.[6−9] More recently, we have demonstrated attachment to Si via both thiol and selenol groups.[10] We have also reported a new attachment method that not only affords facile attachment to Si via Group VI atoms, but also expands the pool of linking atoms to carbon.[11] Ready access to electroactive species tethered to Si via S−Si,

[†] Department of Chemistry, University of California, Riverside.
[‡] Department of Chemistry, North Carolina State University.

(1) Meindl, J. D.; Chen, Q.; Davis, J. A. *Science* **2001**, *293*, 2044−2049.
(2) Joachim, C.; Gimzewski, J. K.; Aviram, A. *Nature* **2000**, *408*, 541−548.
(3) Kwok, K. S.; Ellenbogen, J. C. *Mater. Today* **2002**, *5*, 28−37.
(4) Tseng, G. Y.; Ellenbogen, J. C. *Science* **2001**, *294*, 1293−1294.
(5) Roth, K. M.; Dontha, N.; Dabke, R. B.; Gryko, D. T.; Clausen, C.; Lindsey, J. S.; Bocian, D.F.; Kuhr, W. G. *J. Vac. Sci. Technol. B* **2000**, *18*, 2359−2364.
(6) Li, Q.; Mathur, G.; Gowda, S.; Surthi, S.; Zhao, Q.; Yu, L.; Lindsey, J. S.; Bocian, D. F.; Misra, V. *Adv. Mater.* **2004**, *16*, 133−137.
(7) Roth, K. M.; Yasseri, A. A.; Liu, Z.; Dabke, R. B.; Malinovskii, V.; Schweikart, K.-H.; Yu, L.; Tiznado, H.; Zaera, F.; Lindsey, J. S.; Kuhr, W. G.; Bocian, D. F. *J. Am. Chem. Soc.* **2003**, *125*, 505−517.
(8) Li, Q.; Surthi, S.; Mathur, G.; Gowda, S.; Misra, V.; Sorenson, T. A.; Tenent, R. C.; Kuhr, W. G.; Tamaru, S.-i.; Lindsey, J. S.; Liu, Z.; Bocian, D. F. *Appl. Phys. Lett.* **2003**, *83*, 198−200.
(9) Li, Q.; Mathur, G.; Homsi, M.; Surthi, S.; Misra, V.; Malinovskii, V.; Schweikart, K.-H.; Yu, L.; Lindsey, J. S.; Liu, Z.; Dabke, R. B.; Yasseri, A.; Bocian, D. F.; Kuhr, W. G. *Appl. Phys. Lett.* **2002**, *81*, 1494−1496.
(10) Balakumar, A.; Lysenko, A. B.; Carcel, C.; Malinovskii, V. L.; Gryko, D. T.; Schweikart, K.-H.; Loewe, R. S.; Yasseri, A. A.; Liu, Z.; Bocian, D. F.; Lindsey, J. S. *J. Org. Chem.* **2004**, *69*, 1435−1443.
(11) Liu, Z.; Yasseri, A. A.; Loewe, R. S.; Lysenko, A. B.; Malinovskii, V. L.; Zhao, Q.; Surthi, S.; Li, Q.; Misra, V.; Lindsey, J. S.; Bocian, D. F. *J. Org. Chem.* **2004**, 69, 5568−5577.

Se−Si−, and C−Si bonds affords the possibility of exploring how the different linkages affect the physical characteristics of the surface-bound species.

In the present study, we examine the structural and electron-transfer characteristics of a series of porphyrinic molecules covalently linked to Si(100) via O, S, and Se anchors. To the best of our knowledge, this is the first detailed study of organo-thiols and organo-selenols bound to Si. In contrast, there are hundreds (if not thousands) of studies of organo-thiols on Au and other substrates.[12] A few studies of the organo-selenols on Au have also been reported.[13−17] The particular motivation for this work stems from prior experimental and theoretical studies on the conductivity of molecular wire systems with different Group VI "alligator clips" for attachment to Au.[18−23] Those studies yielded contradictory results as to whether the conductivity is significantly different through O versus S versus Se attached species.[19] Our ability to prepare porphyrins bound to Si using all three types of Group VI atoms allowed us to perform a systematic study aimed at understanding the relative rates of electron-transfer with the three different types of linkers.

Herein, we examine members of two classes of Zn porphyrin monolayers on Si(100). The molecules, designated as **ZnPBzX**− and **ZnPCH$_2$X**−, contain either a benzyl (−**Bz**−) or methylene (−**CH$_2$**−) unit terminated with a Group VI atom (X = O, S, Se) appended to a *meso*-position of the porphyrin, with the nonlinking meso-substituents consisting of either mesityl (−**Bz**− class) or *p*-tolyl and phenyl (−**CH$_2$**− class) units (Chart 1).[10] The O-functionalized porphyrins were prepared from hydroxy species, whereas the S- and Se-functionalized molecules were prepared from *S*-acetylthio or *Se*-acetylseleno protected species. The protecting groups were used for convenience, and do not affect the nature of the final monolayers because it is known that such protecting groups undergo cleavage during the attachment procedure.[10] Two other OH-terminated porphyrins were also included in the studies as controls (Chart 1). These porphyrins include a member of the −**Bz**− class with *p*-tolyl nonlinking substituents (*tol*-**ZnPBzO**−) and a member of the −**CH$_2$**− class with mesityl nonlinking substituents (*mes*-**ZnPCH$_2$O**−).

The two series of **ZnPBzX**− and **ZnPCH$_2$X**− monolayers on Si(100) were examined using a variety of techniques, including X-ray photoelectron spectroscopy (XPS), Fourier transform infrared (FTIR) spectroscopy, and various electrochemical methods, including fast scan cyclic voltammetry and swept waveform AC voltammetry (SWAV). The XPS studies were used to survey the characteristics of the adsorbate binding via the O, S, or Se atoms to the Si surface, whereas the FTIR experiments were used to measure the relative orientations of the porphyrinic rings with respect to the surface plane. Both XPS and voltammetric measurements were employed to quantitate the packing densities of the monolayers. The SWAV measurements were made to elucidate the kinetics of electron transfer for the different types of molecules. Collectively, the studies reported herein expand on our previous work of **ZnPBzO**− monolayers on Si(100),[7] and provide a detailed picture of how the nature of the anchor atom and the linker type influence the structural and electron-transfer characteristics of these general classes of monolayers.

Chart 1

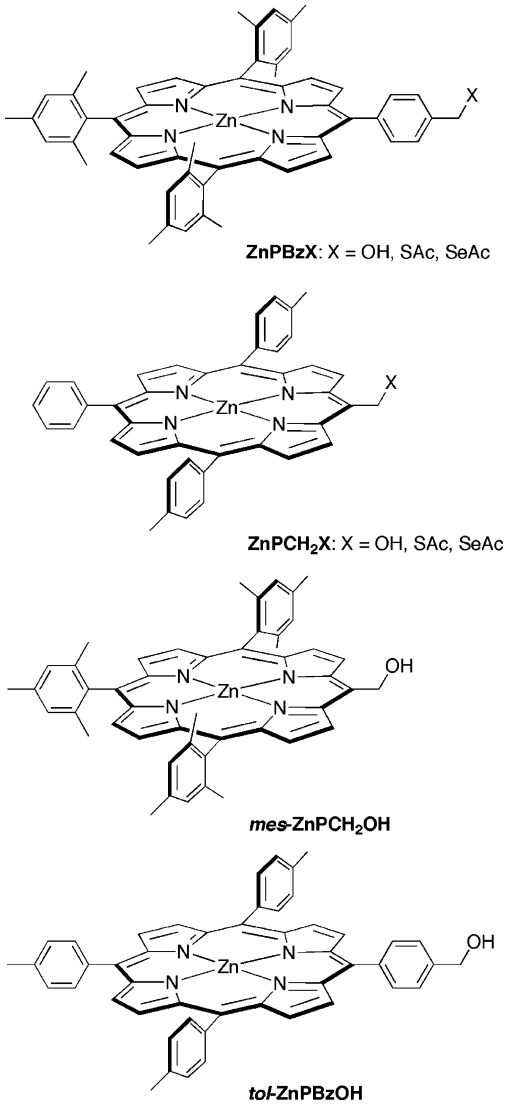

II. Experimental Section

A. Materials. The porphyrins **ZnPBzX** (*X* = hydroxy,[7] *S*-acetylthio,[10] *Se*-acetylseleno[10]), **ZnPCH$_2$X** (*X* = hydroxy, *S*-acetylthio, *Se*-acetylseleno),[24] and *mes*-**ZnPBzOH**[24] were prepared as previously reported. The preparation of *tol*-**ZnPCH$_2$OH** is described in the Supporting Information.

(12) Ulman, A. *Chem. Rev.* **1996**, *96*, 1533−1554.
(13) Han, S. W.; Kim, K. *J. Colloids Interface Sci.* **2001**, *240*, 492−497.
(14) Bandyopadhyay, K.; Vijayamohanan, K.; Venkataramanan, M.; Pradeep, T. *Langmuir* **1999**, *15*, 5314−5322.
(15) Huang, F. K.; Horton, R. C., Jr.; Myles, D. C.; Garrell, R. L. *Langmuir* **1998**, *14*, 4802−4808.
(16) Dishner, M. H.; Hemminger, J. G.; Feher, F. J. *Langmuir* **1997**, *13*, 4788−4790.
(17) Samant, M. G.; Brown, C. A.; Gordon, J. G., II *Langmuir* **1992**, *8*, 1615−1618.
(18) Yaliraki, S. N.; Kemp, M.; Ratner, M. A. *J. Am. Chem. Soc.* **1999**, *121*, 3428−3434.
(19) Patrone, L.; Palacin, S.; Bourgoin, J. P.; Lagoute, J.; Zambelli, T.; Gauthier, S. *Chem. Phys.* **2002**, *281*, 325−332.
(20) Di Ventra, M.; Lang, N. D.; Pantelides, S. T. *Chem. Phys.* **2002**, *281*, 189−198.
(21) Hong, S.; Reifenberger, R.; Tian, W.; Datta, S.; Henderson, J.; Kubiak, C. P. *Superlatt. Microstruct.* **2000**, *28*, 289−303.
(22) Seminario, J. M.; Zacarias, A. G.; Tour, J. M. *J. Am. Chem. Soc.* **1999**, *121*, 411−416.
(23) Reinerth, W. A.; Burgin, T. P.; Dunbar, T. D.; Bumm, L. A.; Arnold, J. J.; Jackiw, J. J.; Zhou, C.-w.; Deshpande, M. R.; Allara, D. L.; Weiss, P. S.; Reed, M. A.; Tour, J. M. *Book of Abstracts, 215th ACS National Meeting, Dallas, March 29-April 2* 1998, PMSE−124.
(24) Carcel, C. M.; Laha, J. K.; Loewe, R. S.; Thamyongkit, P.; Schweikart, K.-H.; Misra, V.; Bocian, D. F.; Lindsey, J. S. *J. Org. Chem.*, in press.

The anhydrous solvents employed in the preparation of the monolayers and in the electrochemical measurements include benzonitrile (Aldrich, 99%), CH_2Cl_2 (Aldrich, 99.8%), and propylene carbonate (PC) (Aldrich, 99.7%), which were used as received. The Bu_4NPF_6 (Aldrich) supporting electrolyte was recrystallized three times from methanol (Fisher), dried under vacuum over a period of several days, and maintained under an inert atmosphere (glovebox) until used.

Silicon wafers (Silicon Valley Microelectronics) were purchased as both thermally oxidized B-doped Si(100) ($\rho = 0.01-0.03\ \Omega$ cm) and non-oxidized B-doped Si(100) ($\rho = 10-30\ \Omega$ cm) for electrochemical and spectroscopic experiments, respectively. The use of high resistivity Si(100) ($\rho = 10-30\ \Omega$ cm) was required for the FTIR experiments to minimize infrared absorption by the charge carriers in the bulk. The chemicals used in Si microelectrode fabrication were AZ 5214 (positive photoresist, Baker), AZ 400K (photoresist developer, Baker), Baker Aleg-355 (resist stripper, Baker), Nanostrip (Cyantek), HF dip (5:1) (Baker), Buffered Oxide Etch (10:1) (Baker), and Baker Clean JTB-111 (Baker). Ar and N_2 (99.995%) were passed through Drierite (Fisher) and Oxyclear (Supelco) gas purifiers prior to use. Deionized water (from a Milli-Q system) had a $\rho \geq 16$ MΩ cm.

B. Electrode Fabrication. 1. Si(100) Microelectrodes. The electrochemical measurements on the monolayers were made using highly doped *p*-type Si(100) working microelectrodes ($100 \times 100\ \mu$m) fabricated as previously described.[7] Each microelectrode was cleaned and hydride terminated using a pre-sparged 1% HF solution.[7] The electrodes were then immediately rinsed, blown dry with N_2 (99.999%), and sealed in VOC vials using a septum fitted cap, purged for 10 min with Ar, and heated to 400 °C for an additional 2 min while the Ar purge was maintained. This process proved effective in removing most residual oxygen species from the silicon surface, as indicated by the absence of surface oxide in the XPS and FTIR spectra of the bulk Si surface.[25] XPS survey spectra on a series of hydride terminated sample blanks reproducibly indicated the presence of residual O and C surface impurities, but those most likely originate from adsorption of adventitious hydrocarbons and/or physisorption of water during the time of sample transfer into the XPS chamber. IR spectroscopy indicated the presence of mono-, di-, and tri-hydride species,[26] which are consistent with a somewhat atomically roughened surface (~5 Å based on our previous AFM measurements[7]).

2. Counter/Reference Electrode. For the electrochemical experiments on the monolayers, a bare silver wire (Ag/Ag^+) served as the counter/reference electrode in a two-electrode setup as described in detail elsewhere.[7] The electrode was prepared by polishing the surface of the Ag wire (Goodfellow), washing it with deionized water, sonicating it in acetone and rinsing it with propylene carbonate containing 1.0 M Bu_4NPF_6. The prepared Ag wire was placed inside a 10 μL polypropylene disposable pipet tip containing ~2 μL of the propylene carbonate/1.0 M Bu_4NPF_6 electrolyte solution and manipulated using a micropositioning device in a setup previously illustrated elsewhere.[7]

C. Monolayer Preparation. All of the **ZnPBzX**− and **ZnPCH$_2$X**− monolayers on Si(100) were prepared using a high-temperature (400 °C), short-time (2 min) "baking" attachment procedure recently developed in our laboratory and described in detail elsewhere.[11] The surface coverage and conditions for achieving saturation coverage were determined electrochemically in a series of experiments wherein the concentration of the porphyrin in the deposition solution (benzonitrile) was systematically varied. These experiments revealed that the surface coverage could be varied in a controlled fashion from the low 10^{-12} mol cm^{-2} to the mid 10^{-11} mol cm^{-2} range (saturation coverage) by varying the porphyrin concentration from ~2 μM to ~2 mM.

The monolayers for the electrochemical experiments were prepared by dispensing a 2 μL drop of the porphyrin solution onto the surface of the microelectrode contained in a sparged VOC vial sealed under Ar. The monolayers prepared for the XPS and FTIR experiments utilized much larger platforms (~1 cm^2), and consequently required a layer drop size, ~50 μL. After deposition, the vial containing the Si substrate was heated on a hotplate at 400 °C for 2 min, and then removed and purged with Ar until cooling to room temperature. Finally, the Si substrate was rinsed and sonicated five times with anhydrous CH_2Cl_2 and purged dry once again under Ar.

D. XPS Measurements. The XPS data were collected using a Leybold EA11-MCD system equipped with a Mg−Kα X-ray (1253.6 eV) source, a hemispherical analyzer, and an 18-multichannel detector. The main XPS chamber was maintained at a steady base pressure of $< 3 \times 10^{-8}$ Torr. The samples were introduced through an intermediate pumping stage by using a fast-transfer mechanical moving rod, a procedure that required a total time of approximately 5 min. All spectra were obtained using identical data collection parameters. Survey (scans of 1000 eV or more) and high-resolution spectra were obtained by averaging over 10 or 50 scans and using average dwell times of 100 or 250 ms per point and scan, respectively. Survey spectra were obtained with a band-pass energy of 100.8 eV and an ~1 mm entering aperture, which correspond to a spectral resolution of ~1.5 eV. High-resolution spectra were obtained with a band-pass energy of 31.5 eV, which corresponds to a spectral resolution of ~0.8 eV. High-resolution spectra were collected for the Si 2p, Zn $2p_{3/2}$, N 1s, S 2s, and Se 3d XPS peaks for the blank hydride terminated Si(100) surface and for all **ZnPBzX**− and **ZnPCH$_2$X**− monolayers. To compensate for any potential surface charging effects, all the XPS peak positions were referred to the residual adventitious hydrocarbon C 1s peak at 284.6 eV. The spectra from the high-resolution scans were fit to Gaussian peaks after background subtraction using Analytics software for quantitative analysis. The binding energies for the surface-bound adsorbates were found to be reproducible to within an experimental error of about ±0.1 eV, and the relative intensities to within 10−15%. In the case of the Zn $2p_{3/2}$, N 1s, S 2s, and Se 3d, the peak fits were constrained such that the same parameters, peak positions, and widths were used for the different porphyrin monolayers.

E. FTIR Spectroscopy. The FTIR spectra of the porphyrins in both solid and monolayer forms were collected at room temperature using a Bruker Tensor 27 FTIR spectrometer. In all cases, a spectral resolution of 4 cm^{-1} was used. The spectra of the solid porphyrin samples were obtained in KBr pellets (~1−2 wt % porphyrin). These spectra were collected in transmission mode using a room-temperature DTGS detector by averaging over 32 scans.

The IR spectra of the Si−H$_x$ and porphyrin-modified Si(100) surfaces were obtained using a Harrick Scientific horizontal reflection Ge attenuated total reflection accessory (GATR, 65° incidence angle). The Si substrates were placed in contact with the flat surface of a semispherical Ge crystal that serves as the optical element, and IR spectra were collected with p polarized light using a liquid-nitrogen cooled medium-bandwidth MCT detector (600−4000 cm^{-1}) and averaging over 256 scans. The IR spectra of the Si−H$_x$ surface were obtained as the ratio of the single beam spectrum of the HF-etched Si(100) surface against that of a Si(100) sample with a native oxide film. The spectra of the porphyrin monolayers were referenced against that of a Si−H$_x$ surface previously subjected to the same deposition conditions as those used to obtain the monolayer but using only the neat deposition solvent. The Ge crystal was cleaned with neat 2-butanone before every experiment, and the GATR accessory was purged with dry N_2 during data acquisition.

F. Electrochemical Measurements. The electrochemical measurements of the porphyrins in solution were made in a standard three-electrode cell using Pt working and counter electrodes and a Ag/Ag^+ reference electrode. The solvent/electrolyte was CH_2Cl_2 containing 1.0 M Bu_4NPF_6. The electrochemical measurements on the monolayers were performed in a two electrode configuration using the fabricated Si(100) microelectrode and the Ag counter/reference electrode described

(25) Grundner, M.; Jacob, H. *Appl. Phys. A* **1986**, *A39*, 73−82.
(26) Chabal, Y. J.; Raghavachari, K. *Phys. Rev. Lett.* **1985**, *54*, 1055−1058.

earlier.[7] The solvent/electrolyte was propylene carbonate containing 1.0 M Bu_4NPF_6. The RC time constant for the microelectrode/electrochemical cell was measured to be ~3 μs, which is sufficiently short to preclude any significant interference with the measurement of the electron-transfer rates. Cyclic voltammograms were recorded in a 0−1.4 V potential window with a CH Instruments Model 600A Electrochemical Analyzer. The surface coverage of the porphyrins in the monolayer was determined by integration of the total charge in the first anodic wave and by using the geometric dimensions of the microelectrode. The standard electron-transfer rate constants of the porphyrin monolayers were obtained using a swept waveform AC voltammetry (SWAV) method described and tested in detail in previous work.[7,27]

III. Results

A. XPS Studies. The XPS signatures of the saturation-coverage porphyrin monolayers were examined to characterize their binding mode to the Si(100) substrate. Representative photoelectron spectra of the **ZnPBzX**− and **ZnPCH$_2$X**− monolayers are shown in Figures 1 and 2, respectively, and data extracted from those spectra are summarized in Table 1. Porphyrin modification of the surface is indicated both by the appearance of new photoelectron signals for the elements in the porphyrin macrocycle (Zn, and/or N) and its atomic anchor units (O, S, or Se), and by the attenuation of the bulk signature peaks from the Si surface. Specifically, porphyrin Zn 2p$_{3/2}$ and N 1s XPS signals are observed in all cases at ~1021 eV and ~398 eV, respectively.[7,28,29] Moreover, the sharp S 2s and Se 3d XPS peaks (Figures 1 and 2, insets) suggest a single type of derivatization of the Si(100) surface. The binding energies of S (227.3 eV) and Se (54.9 eV) atoms in the porphyrin monolayers are in good agreement with those previously reported for benzenethiol on Si[30] and diphenyl diselenide on Au,[14] and no evidence is seen for multiple bands to indicate the presence of physisorbed molecules.[31−33]

Quantitative analysis of the spectra was also carried out by scaling the spectral intensity of the elements of interest (Zn, N, and bulk Si) using known atomic cross-section sensitivity factors.[34] The N:Zn atomic ratios were found to be in good agreement with the expected value of 4:1 (N:Zn) for the porphyrin (data not shown). The value of the Zn:Si atomic ratio and the intensity of the Si signal obtained from the clean Si−H_x surface before derivatization were used to estimate the surface concentration (Γ) for each monolayer (assuming homogeneous coverage) (Table 1). These estimates of surface concentration assumed no attenuation of Zn photoelectrons by the surrounding porphyrin. More accurate values of the surface concentration were determined electrochemically (vide infra).

The average thickness (T) of the **ZnPBzX**− and **ZnPCH$_2$X**− monolayers was also estimated from the XPS data (Table 1) by assuming monolayer uniformity within the underlying substrate and using a mean free path of ~33 Å for the Si 2p photoelectrons through the adsorbed organic film at the experimental take off angle of 15° (estimated from previously reported values).[35] The average thicknesses of the three types of **ZnPBzX**− monolayers were found to be quite similar, ~18 ± 1 Å, and likewise, the average thicknesses of the three types of **ZnPCH$_2$X**− monolayers are also similar, but lower than those of the **ZnPBzX**− monolayers, ~13 ± 1 Å. These values can be compared with a previously reported value for free base tetraphenylporphyrin of 17.6 Å.[35] The average thickness for both the **ZnPBzX**− and **ZnPCH$_2$X**− monolayers is less than that expected for a molecule standing upright on the surface, and indicate a tilted orientation instead. This molecular tilt was confirmed by the FTIR studies (vide infra).

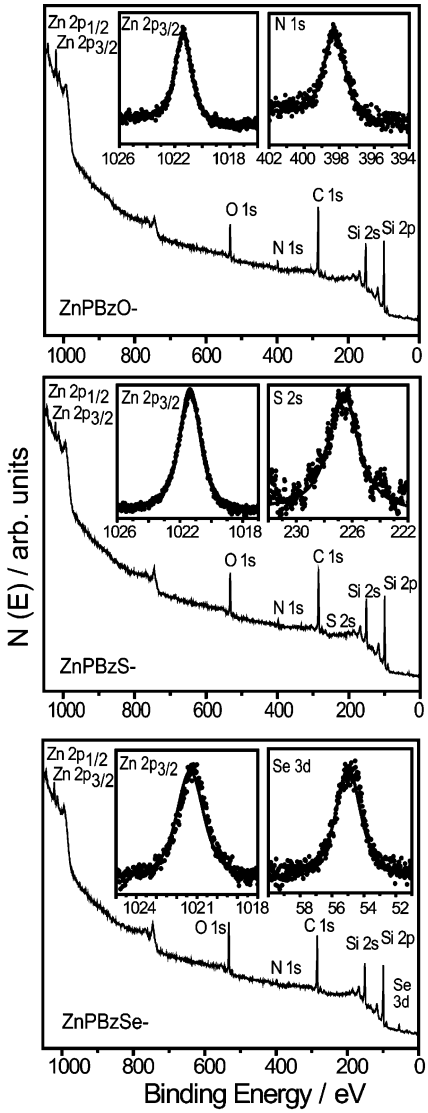

Figure 1. Survey X-ray photoelectron spectra (XPS) of saturation-coverage **ZnPBzX**− monolayers on Si(100). Insets: High-resolution scans for the Zn 2p$_{3/2}$, S 2s and Se 3d spectral regions showing both the raw data (dots) and Gaussian fits (solid lines).

B. FTIR Studies. A series of FTIR studies was conducted to investigate the structure of the porphyrins and the adsorption geometry in the monolayers. The mid-frequency (700−1800

(27) Roth, K. M.; Gryko, D. T.; Clausen, C.; Li, J.; Lindsey, J. S.; Kuhr, W. G.; Bocian, D. F. *J. Phys. Chem. B* **2002**, *106*, 8639−8648.
(28) Polzonetti, G.; Ferri, A.; Russo, M. V.; Iucci, G.; Licoccia, S.; Paolesse, R. *J. Vac. Sci. Technol. A* **1999**, *17*, 832−839.
(29) Zhang, Z.; Hu, R.; Liu, Z. *Langmuir* **2000**, *16*, 1158−1162.
(30) Coulter, S. K.; Schwartz, M. P.; Hamers, R. J. *J. Phys. Chem. B* **2001**, *105*, 3079−3087.
(31) Yasseri, A. A.; Syomin, D.; Malinovskii, V. L.; Loewe, R. S.; Lindsey, J. S.; Zaera, F.; Bocian, D. F. *J. Am. Chem. Soc.* **2004**, *126*, 11944−11953.
(32) Zak, J.; Yuan, H.; Ho, M.; Woo, L. K.; Porter, M. D. *Langmuir* **1993**, *9*, 2772−2774.
(33) Hutchison, J. E.; Postlethwaite, T. A.; Murray, R. W. *Langmuir* **1993**, *9*, 3277−3283.
(34) Wagner, C. D.; Riggs, W. M.; Davis, L. E.; Moulder, J. F.; Muilenberg, G. E. *Handbook of X-ray Photoelectron Spectroscopy*; Perkin-Elmer Corporation: Eden Prairie, 1978.
(35) Boeckl, M. S.; Bramblett, A. L.; Hauch, K. D.; Sasaki, T.; Ratner, B. D.; Rogers, J. W., Jr. *Langmuir* **2000**, *16*, 5644−5653.

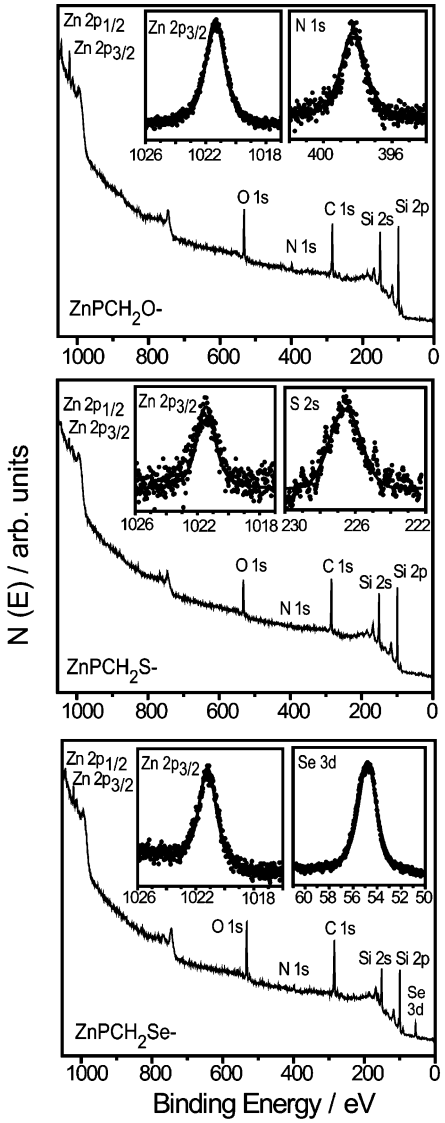

Figure 2. Survey XPS spectra of saturation-coverage **ZnPCH$_2$X**− monolayers on Si(100). Insets: High-resolution scans of the Zn 2p$_{3/2}$, S 2s and Se 3d spectral regions showing both the raw data (dots) and Gaussian fits (solid lines).

Table 1. XPS Data for the **ZnPBzX**− and **ZnPCH$_2$X**− (X = O, S, Se) Monolayers on Si(100)

	binding energy/ ± 0.1 eV					atomic ratio[a]		
	Si	Zn	N	S	Se	Zn:Si	Γ/10^{-11} [b]	T[c]
monolayer	2 p	2 p$_{3/2}$	1 s	2 s	3 d	2 p$_{3/2}$:2 p	mol cm^{-2}	Å
ZnPBzO-	99.4	1021.3	398.4			0.055	6.2	19
ZnPBzS-	99.4	1021.4	398.3	227.4		0.045	5.1	17
ZnPBzSe-	99.4	1021.2	397.9		55.0	0.044	5.0	18
ZnPCH$_2$O-	99.5	1021.3	398.3			0.061	6.8	13
ZnPCH$_2$S-	99.5	1021.5	398.2	227.3		0.051	5.8	12
ZnPCH$_2$Se-	99.5	1021.1	398.2		54.8	0.068	7.6	12

[a] Calculated using reported atomic sensitivity factors for Zn p$_{3/2}$ and Si 2p, and corrected for the kinetic dependence of the spectrometer detection efficiency. An uncertainty of ± 0.001 was estimated based on three different **ZnPBzO**− samples. [b] Porphyrin surface concentrations,based on a surface atomic density for Si(100) of 6.78 × 10^{14} atoms cm^{-2}. [c] Film thickness, measured using the ratio of the substrate signal (I_{Si}) to that of pure silicon hydride (I_{SiH}), $T = -\lambda\ (E_{Si})\ \cos\ (15°)\ \ln(I_{Si}/I_{SiH})$,[35,55] with $\lambda\ (E_{Si}) \approx 33$ Å.

cm^{-1}) IR spectra of solid samples of the parent **ZnPBzX** and **ZnPCH$_2$X** porphyrins (with their OH, *S*-AcS, and *Se*-AcSe terminal groups intact) are shown for comparison in the top of each pair of traces in Figures 3 and 4, respectively. The spectra exhibit numerous bands in this frequency region, which previous studies of structurally related porphyrins have shown to be due mostly to in-plane modes of the porphyrin ring or the aryl substituents, one of the most prominent features being the porphyrin pyrrole ring breathing mode near 998 cm^{-1}.[36] The only salient feature due to an out-of-plane mode of the porphyrin is the band at 797 cm^{-1}, which is due to a β-pyrrole hydrogen deformation.[37] For the porphyrins that contain *S*-AcS or *Se*-AcSe protecting groups, other relevant features are observed in the 1685−1715 cm^{-1} region associated with the carbonyl stretching vibration (ν(C═O)) of the acetyl protecting group. In the high-frequency (2600−3400 cm^{-1}) spectral region (not shown), only weak bands are observed, all attributable to C-H (or O−H) stretches.

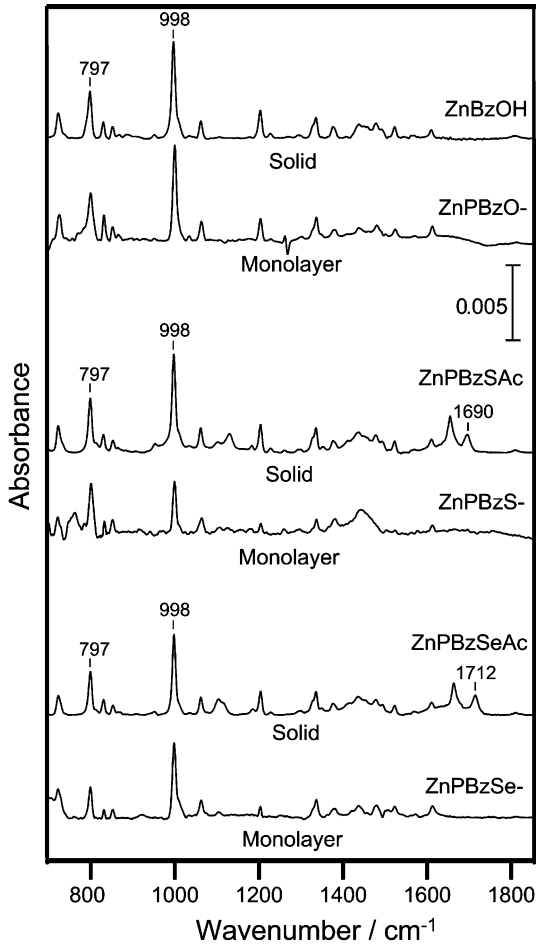

Figure 3. Fourier transform infrared (FTIR) spectra of the **ZnPBzX** porphyrins both in solid form and as monolayers on Si(100). The terminal groups (X) in the solid porphyrins are OH, *S*-AcS, or *Se*-AcSe.

The corresponding IR spectra of the saturation-coverage **ZnPBzX**− and **ZnPCH$_2$X**− monolayers are shown in the bottom of each pair of traces in Figures 3 and 4, respectively. The spectra of all the monolayers are plotted on the same absolute intensity scale to allow for the comparison of the relative intensities of the bands. The key features observed in the IR spectra of the monolayers are as follows:

(36) Li, X. Y.; Czernuszewicz, R. S.; Kincaid, J. R.; Su, Y. O.; Spiro, T. G. *J. Phys. Chem.* **1990**, *94*, 31−47.
(37) Li, X. Y.; Czernuszewicz, R. S.; Kincaid, J. R.; Spiro, T. G. *J. Am. Chem. Soc.* **1989**, *111*, 7012−7023.

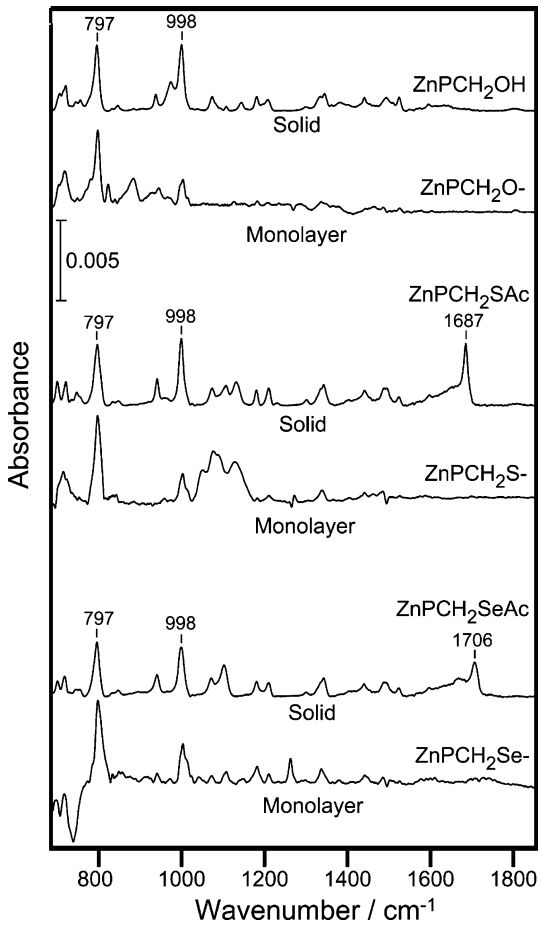

Figure 4. FTIR spectra of the **ZnPCH$_2$X** porphyrins both in solid form and as monolayers on Si(100). The terminal groups (X) in the solid porphyrins are OH, *S*-AcS, or *Se*-AcSe.

(1) The spectra for the monolayer and solid samples of a given type of porphyrin are quite similar. This indicates that the structure of the porphyrin macrocycle and substituent groups is retained upon monolayer formation.

(2) The bands associated with the ν(C═O) modes (1685−1715 cm^{-1}) are absent from the spectra of the monolayers of the thiol and selenol-terminated porphyrins, indicating the cleavage of this group upon monolayer formation.[31]

(3) The relative IR intensities of the in-plane (e.g., 998 cm^{-1}) versus out-of-plane (797 cm^{-1}) porphyrin modes are different for the monolayers versus solids. These differences are most apparent for the **ZnPCH$_2$X** class of porphyrins (Figure 4), and indicate a preferred ordered orientation of the adsorbed molecules with respect to the plane of the surface.

The relative intensities of the in-plane and out-of-plane porphyrin modes (Table 2) can be used to determine the average tilt angle (α) of the porphyrin ring with respect to the surface normal.[38−40] The evaluation of this average tilt angle is predicated on certain assumptions. (1) The porphyrin ring is planar, and thus the 998 and 797 cm^{-1} modes are pure in-plane and out-of-plane vibrations, respectively. This assumption is reasonable considering that Zn tetraphenylporphyrin is planar.[41] (2) The magnitude of the intrinsic transition-dipole moments of the porphyrin vibrations in the randomly oriented solid phase are similar to those in the surface-bound monolayer. (3) The orientation of the porphyrin ring can be described by a single angle, the average tilt (azimuthal) angle from the surface normal. Two more angles are in principle needed to fully determine adsorption geometries, the polar angle around the surface normal (assumed here to be random), and the rotation around the main molecular axis (fixed here at 0° with respect to the surface plane. Preliminary work in our lab suggests that this angle may vary from 0°, but that this variation may not significantly affect the estimate of the azimuthal angle reported below). Under these assumptions, the average tilt angle for the porphyrins in the monolayers was determined from the ratios of the relative intensities of the in-plane and out-of-plane porphyrin modes in the monolayers versus the solids using standard methods.[42,43] The average angles determined from the IR data for the saturation-coverage porphyrin monolayers are reported in Table 2.

Table 2. FTIR Relative Intensities and Adsorption Geometries for the **ZnPBzX**− and **ZnPCH$_2$X**− (X = O, S, Se) Monolayers on Si(100)

monolayer	FTIR intensity ratios[a] (I_s^{797}/I_s^{998})	FTIR intensity ratios[a] (I_m^{797}/I_m^{998})	tilt, α[b] (deg)	T[c] Å
ZnPBzO−	0.48	0.44	34	17
tol-**ZnPBzO**−	0.95	0.89	34	17
ZnPBzS−	0.55	0.94	43	15
ZnPBzSe−	0.52	0.51	35	17
ZnPCH$_2$O−	0.98	3.4	53	10
mes-**ZnPCH$_2$O**−	0.52	1.03	55	12
ZnPCH$_2$S-	0.93	3.1	52	11
ZnPCH$_2$Se-	1.1	2.1	44	12

[a] Intensity ratio of the out-of-plane β-pyrrole hydrogen deformation (797 cm^{-1}) mode and the in-plane pyrrole breathing (998 cm^{-1}) band for the porphyrins in solids (s) versus monolayers (m). [b] Tilt (azimuthal) angle of adsorbed porphyrins with respect to the surface normal. [c] Film thickness, calculated from the tilt angles and the average molecular lengths, 20 and 17 Å for **ZnPBzX**- and **ZnPCH$_2$X**- respectively.

Inspection of Table 2 reveals that although the average tilt angles determined for the different types of monolayers vary somewhat among the molecules, the α values for the −**Bz**− class are on average noticeably less ($\alpha_{Bz} \sim 37°$) than those for the −**CH$_2$**− class ($\alpha_{CH_2} \approx 50°$). Interestingly, the average tilt angles for the **ZnPBzX**− and **ZnPCH$_2$X**− monolayers are in the same range as that previously determined for porphyrins tethered to Si via a tripodal siloxane linker ($\alpha \approx 43 \pm 3°$).[44] To investigate whether the nonlinking substituent groups (mesityl versus *p*-tolyl and phenyl, see Chart 1) play any role in determining the tilt angle values, additional FTIR spectra were obtained for monolayers of the control *tol*-**ZnPBzO**− and *mes*-**ZnPCH$_2$O**− porphyrins (Chart 1). The relative intensity data and the calculated average tilt angles for these molecules are included in Table 2. It was found that the α values for the control molecules are essentially identical to those of **ZnPBzO**− and **ZnPCH$_2$O**−, respectively. Accordingly, the class of linker (−**Bz**− versus −**CH$_2$**−), as opposed to the type of nonlinking substituent groups (mesityl versus *p*-tolyl and phenyl), appears to be the dominant factor in determining the average tilt angle.

(38) Painter, P. C.; Coleman, M. M.; Koenig, J. L. *The Theory of Vibrational Spectroscopy and Its Application to Polymeric Materials*, 1982.
(39) Allara, D. L.; Nuzzo, R. G. *Langmuir* **1985**, *1*, 52−66.
(40) Harrick, N. J.; Mirabella, F. M. *International Reflection Spectroscopy: Review and Supplement*; Harrick Scientific Corp., New York 1985.
(41) Scheidt, W. R.; Kastner, M. E.; Hatano, K. *Inorg. Chem.* **1978**, *17*, 706−710.
(42) Greenler, R. G. *J. Chem. Phys.* **1966**, *44*, 310−315.
(43) Zaera, F. *Int. Rev. Phys. Chem.* **2002**, *21*, 433−471.
(44) Li, D.; Swanson, B. I.; Robinson, J. M.; Hoffbauer, M. A. *J. Am. Chem. Soc.* **1993**, *115*, 6975−6980.

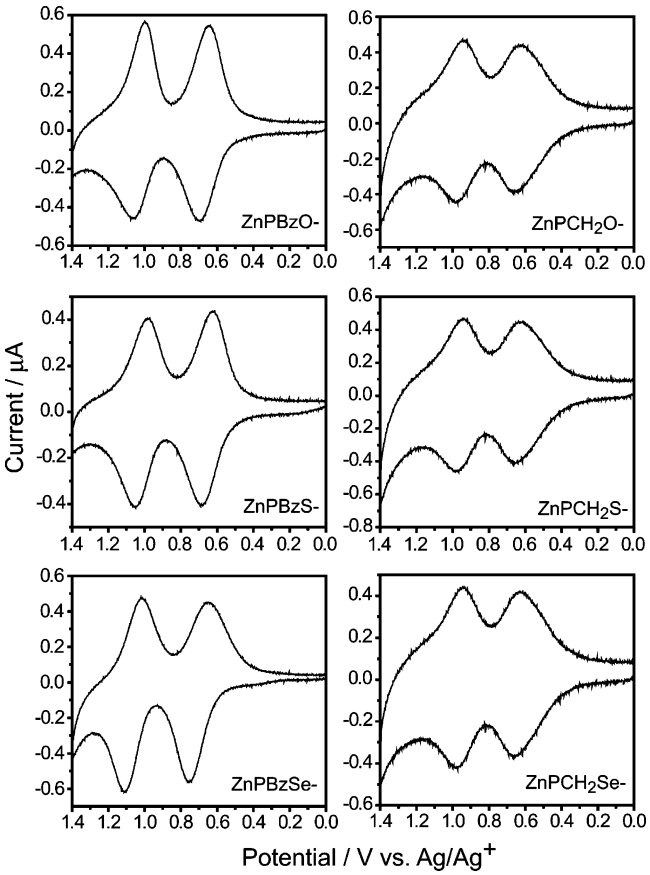

Figure 5. Representative fast-scan (100 V s^{-1}) voltammograms of the **ZnPBzX**− (left column) and **ZnPCH$_2$X**− (right column) monolayers on Si(100).

Finally, the average molecular tilt angles were used in conjunction with their approximate molecular dimensions to estimate the thickness of the monolayers (Table 2). Comparison of the monolayer thicknesses estimated from the IR versus XPS data (Table 1) reveals good agreement between the two measurements.

C. Electrochemical Studies. 1. Voltammetric Characteristics. Representative fast scan (100 V s^{-1}) cyclic voltammograms of the saturation-coverage **ZnPBzX**− and **ZnPCH$_2$X**− monolayers on Si(100) microelectrodes are shown in the left and right columns of Figure 5, respectively. At oxidizing potentials, each monolayer exhibits two resolved voltammetric waves indicative of the formation of mono- and dication porphyrin π-radicals. The redox potentials for the different monolayers and the surface concentrations at saturation coverage extracted from those data are summarized in Table 3. For comparison, the redox potentials for the parent porphyrins in solution are also included in Table 3. The salient observations from the voltammetric studies are summarized below:

(1) All of the monolayers exhibit reversible electrochemical behavior over multiple cycles under ambient conditions. However, after extended voltammetric cycling (several hundred cycles), the monolayers degrade slowly. The relative stability of the monolayers depends on the anchoring atom (O > S > Se), with the O-tethered monolayers being more robust than the S- or Se-tethered monolayers. This is qualitatively consistent with the relative strengths of the Si−O versus Si−S bonds (Si−O, ∼109 kcal mol^{-1}; Si−S, ∼54 kcal mol^{-1}).[30,45] It should be noted that the monolayers are far more robust during redox cycling under inert atmosphere conditions. For the **ZnPBzO**− monolayers on Si(100), 10^{12} redox cycles over a period of 60 days are possible.[46]

Table 3. Redox Potentials and Surface Coverage Values for the **ZnPBzX**− and **ZnPCH$_2$X**− (X = O, S, Se) Monolayers on Si(100)

	$E_{0/+1}$[a]		$E_{+1/+2}$[a]			
	soln.	mon.	soln.	mon.	$\Gamma \times 10^{-11}$ [b]	area[c]
monolayer	(V)	(V)	(V)	(V)	mol cm^{-2}	Å^2
ZnPBzO−	0.53	0.67	0.88	1.03	6.9	241
ZnPBzS−	0.57	0.72	0.86	1.02	6.2	268
ZnPBzSe−	0.56	0.70	0.90	1.06	7.4	224
ZnPCH$_2$O−	0.55	0.64	0.89	0.96	5.5	302
ZnPCH$_2$S−	0.60	0.64	0.88	0.96	5.7	291
ZnPCH$_2$Se−	0.57	0.61	0.87	0.96	5.5	302

[a] Monolayer (mon.) potentials were obtained in propylene carbonate containing 1.0 M *n*-Bu_4NPF_6; scan rate = 100 V s^{-1}. Solution (soln.) potentials were obtained in CH_2Cl_2 containing 1.0 M *n*-Bu_4NPF_6; scan rate 0.1 V s^{-1}. Values are referenced vs Ag/Ag^+; $FeCp_2/FeCp_2^+$ = 0.19. [b] Porphyrin surface concentration, calculated from the integrated area of the $E_{0/+1}$ anodic wave, using the geometric area of the microelectrodes (1 × 10^{-4} cm^2). [c] Molecular footprint on the surface, estimated using the values for Γ.

(2) The redox potentials for the porphyrins in all the monolayers are higher than those for the porphyrins in solution. In addition, the potentials for the **ZnPBzX**− monolayers are higher than those for the **ZnPCH$_2$X**− monolayers. In this regard, our previous studies of **ZnPBzO**− monolayers on Si(100),[7] as well as a number of thiol-derivatized porphyrin monolayers on Au,[5,7,27,31,47,48] have shown that the redox potentials are influenced by both packing density and screening from the solvent and counterions. More densely packed or heavily screened monolayers typically exhibit higher redox potentials. The fact that the redox potentials for the **ZnPBzX**− monolayers are higher than those for the **ZnPCH$_2$X**− monolayers is consistent with the fact that the former exhibit somewhat higher saturation coverages than the latter (Table 3). We have also found that the method of surface attachment has some influence on the potentials. The high-temperature method used here results in potentials that are somewhat lower than those observed with a lower-temperature method previously used for monolayer formation.[7]

(3) The voltammetric peaks of the **ZnPBzX**− monolayers are generally much narrower than those for the **ZnPCH$_2$X**− monolayers, indicating that the thermodynamics of the redox process are more homogeneous for the former type of monolayers.

2. Electron-Transfer Characteristics. Standard electron-transfer rate constants, k^0, were measured for the first oxidation process ($E^{0/+1}$) of the **ZnPBzX**− and **ZnPCH$_2$X**− monolayers at a variety of coverages from the low 10^{-12} to mid 10^{-11} mol cm^{-2} range. The interest in this surface-concentration dependence of the electron-transfer rates stems from our previous studies on **ZnPBzO**− monolayers on Si(100),[7] as well as on thiol-derivatized porphyrin monolayers on Au,[27,31] which show that the electron-transfer rates depend on surface coverage. Unfortunately, owing to experimental limitations, the electron-transfer rates could not be measured at very high surface concentrations, i.e., those at or near the saturation coverages.

(45) Choi, C. H.; Liu, D.-J.; Evans, J. W.; Gordon, M. S. *J. Am. Chem. Soc.* **2002**, *124*, 8730−8740.
(46) Liu, Z.; Yasseri, A. A.; Lindsey, J. S.; Bocian, D. F. *Science* **2003**, *302*, 1543−1545.

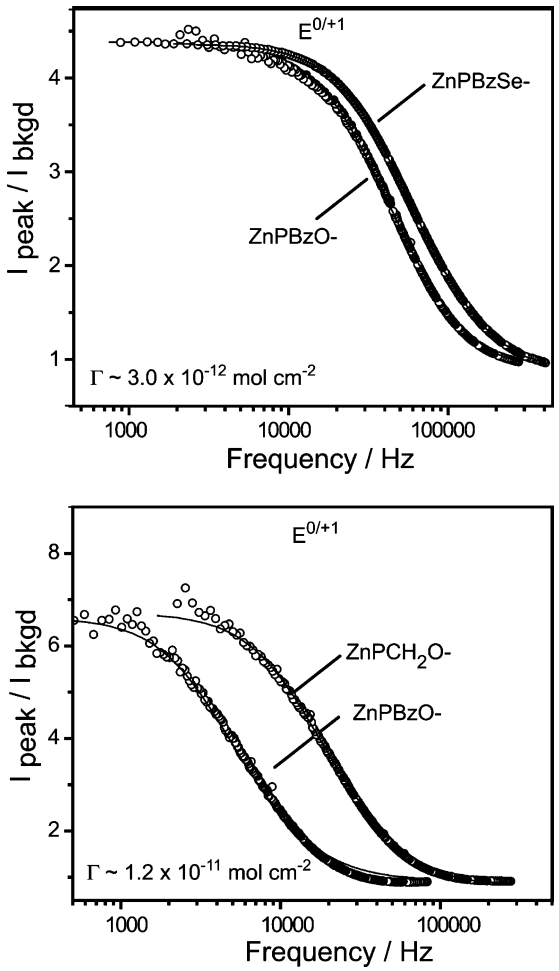

Figure 6. Comparison of I_{peak}/I_{bkdg} versus frequency plots for various **ZnPBzX**− and **ZnPCH$_2$X**− monolayers. Top panel: **ZnPBzO**− and **ZnPBzSe**−; bottom panel: **ZnPBzO**− and **ZnPCH$_2$O**−. The solid curves represent fits of the data using a Randles equivalent circuit model. Fits such as these were used to obtain the k^0 values reported in Figure 7.

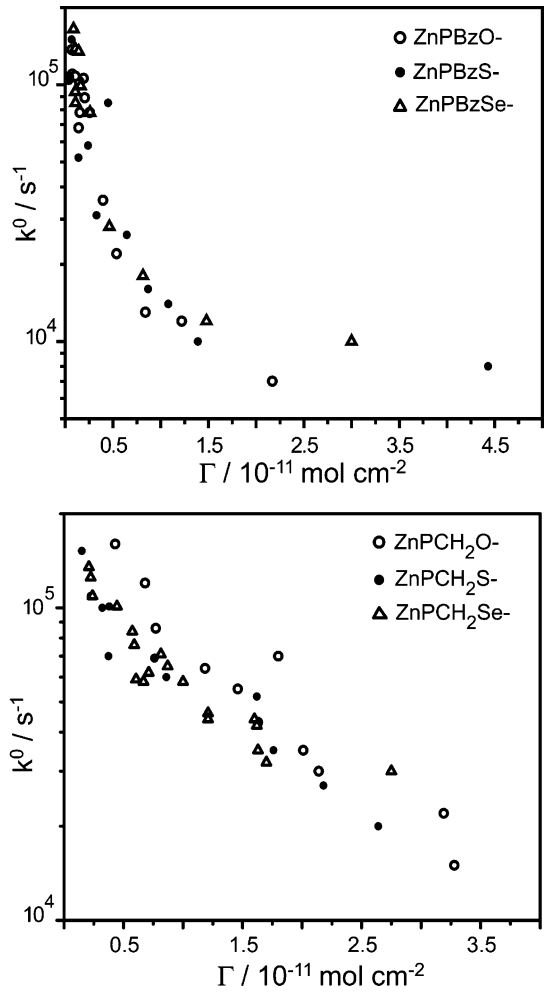

Figure 7. Standard electron-transfer rate constants, k^0, versus surface concentration for the first oxidation process ($E^{0/+1}$) of the **ZnPBzX**− (top panel) and **ZnPCH$_2$X**− (bottom panel) monolayers on Si(100).

Nevertheless, the available concentration range was wide enough to detect significant variations in k^0.

Representative raw data sets used for the determination of k^0 (I_{peak}/I_{bkgd} vs frequency) are shown for **ZnPBzX**− and **ZnPCH$_2$X**− monolayers in Figure 6. The data shown in the top panel compare the frequency role-off curves for the **ZnPBzO**− and **ZnPBzSe**− monolayers measured at approximately the same surface concentration ($\Gamma \approx 3.0 \times 10^{-12}$ mol cm^{-2}), whereas the data shown in the bottom panel compare curves for the **ZnPBzO**− and **ZnPCH$_2$O**− monolayers ($\Gamma \approx 1.2 \times 10^{-11}$ mol cm^{-2}). The key observation from these data is that the rates for the two monolayers with the −**Bz**− class of linker are essentially identical, whereas the rates for the monolayers with the −**CH$_2$**− class of linker are considerably faster. A more systematic discussion of this effect is aided by the plots of k^0 as a function of surface concentration shown for each of the **ZnPBzX**− and **ZnPCH$_2$X**− monolayers in Figure 7 (top and bottom panels, respectively). Inspection of these data reveals again that the electron-transfer rates for the three types of monolayers with the −**Bz**− class linker are similar at any particular surface concentration, and that the same is true for the three types of monolayers with the −**CH$_2$**− class of linker. Also, for both types of monolayers, the k^0 values increase (albeit with different slopes) as the surface concentration decreases, as has been observed in earlier studies on porphyrin monolayers.[7,27,31] Note, however, that the monolayers bearing the −**CH$_2$**− class of linker appear to exhibit faster rates than those with the −**Bz**− class of linker at all surface concentrations, although the distinction is less clear at very low coverages. Collectively, these results indicate that the type of Group VI atom that tethers the porphyrin to the Si surface does not influence the electron-transfer kinetics in any significant way.

IV. Discussion

The studies reported herein on the series of **ZnPBzX**− and **ZnPCH$_2$X**− monolayers permit a systematic exploration of the factors that influence (1) the binding mode of the monolayers to the Si(100) surface, (2) the orientation of the porphyrin rings with respect to the surface plane, and (3) the packing density of the adsorbed layer. These structural properties of the monolayers underpin the thermodynamics and kinetics of their electron-transfer behavior. We address these issues in more detail below.

The first general theme that emerges from our studies is that surface binding can be readily achieved to Si(100) with both relatively short (−**Bz**−) and very short (−**CH$_2$**−) tethers, regardless of the nature of the Group VI anchoring atom (O, S, Se). The longer −**Bz**− class of tethers affords monolayers that

are somewhat more upright on the surface ($\alpha_{Bz} \approx 37°$) than the shorter $-\mathbf{CH_2}-$ tethers ($\alpha_{CH_2} \approx 50°$). The former class of monolayers also exhibit higher packing densities and more homogeneous redox thermodynamics. The fact that the molecules bearing the $-\mathbf{Bz}-$ class of tether stand more upright could be due to a variety of factors. In particular, there could be steric interactions between the phenyl ring of the $-\mathbf{Bz}-$ linker and the surface, perhaps because the phenyl ring cannot become coplanar with the porphyrin macrocycle due to steric constraints.[41] The out-of-plane rotation of the phenyl ring could potentially result in a strong repulsive interaction with the surface. In addition, the $-\mathbf{Bz}-$ tether has more torsional flexibility than the $-\mathbf{CH_2}-$ tether, and could therefore favor a higher degree of interaction between neighboring porphyrins, and hence a higher packing density. In this picture, the more upright orientation for the $-\mathbf{Bz}-$ tethered molecules is an indirect effect of packing rather than a direct effect of phenyl group-surface interactions. It is likely that both effects cited above collectively determine the orientation of the porphyrins on the surface.

The second general theme arising from the studies reported herein is that the kinetics of electron transfer does not depend on the type of Group VI anchoring atom to the Si(100) surface. On the other hand, the type of linker class does affect the electron-transfer rates, especially at intermediate coverages; the monolayers bearing the shorter $-\mathbf{CH_2}-$ class of linker exhibit systematically faster rates than those bearing the $-\mathbf{Bz}-$ linker. This may not be too surprising given that the $-\mathbf{CH_2}-$ class of tether produces monolayers where the porphyrin redox center sits at a shorter distance from the surface. The key question here is why the nature of the Group VI anchoring atom does not affect the electron-transfer rate in any appreciable way. One possible explanation for this may be that the energies of the additional electronic states available in the heavier atoms (Se and S versus O) are higher than the vacuum level of the surface, and therefore do not contribute to the electron-transfer process. On the other hand, it is quite possible that the electron-transfer rates may be controlled by factors other than the nature of the Si−X linker. For example, recent studies of monolayers bearing tethers of different length suggest that Arrhenius prefactors exert limiting effects on electron-transfer kinetics.[49] These limitations occur when the tethers become very short, and are independent of the nature of the linker. However, this explanation is not likely to account for the behavior of **ZnPBzX**− and **ZnPCH$_2$X**− monolayers, because the kinetic limitation cited in that work is observed only at very fast electron-transfer rates, much faster than those observed here. A second possibility is that the electronic characteristics of Si(100) are responsible for the electron-transfer bottleneck. Although we have not fully explored this issue, such an explanation also seems unlikely because, according to some limited studies in our laboratory, the electron-transfer kinetics of the **ZnPZnS**− and **ZnPZnSe**− monolayers on Au(111) appear to display similar rates to those reported herein for the **ZnPZnS**− and **ZnPZnSe**− monolayers on Si(100).

One seemingly more consistent explanation for the similarity in electron-transfer rates for the monolayers anchored with the different Group VI atoms is that the electron-transfer proceeds via a through-space mechanism, and hence the linker and anchoring atom modulate this rate only through changes in surface-redox center distances. In this regard, a through-space process seems more plausible for the very short $-\mathbf{CH_2}-$ tether than for the longer $-\mathbf{Bz}-$ tether. On the basis of the length of the $-\mathbf{CH_2}-$ tether and the average tilt angle of the porphyrin, the distance of closest approach of the edge of the redox center to the surface could be as small as 2−3 Å, as apposed to 5−6 Å for the $-\mathbf{Bz}-$ tether. Regardless, the differences in rates between the monolayers with $-\mathbf{Bz}-$ versus $-\mathbf{CH_2}-$ tethers at any surface concentration are at most a factor of 3 (see Figure 7). Electron-transfer rates fall off exponentially with distance, $\exp(-\beta r)$, and any reasonable value of the constant β for through-space electron transfer ($\beta \approx 1.5-2$ Å^{-1}) would result in a much larger difference between the electron-transfer rates for the molecules with the $-\mathbf{Bz}-$ versus $-\mathbf{CH_2}-$ class.

Perhaps the most likely explanation for the similarity in electron-transfer rates for the monolayers anchored with the different Group VI atoms is that the rate-limiting step is associated with screening effects at the interface between the monolayer and the solvent/electrolyte. In this regard, it is well-established that redox kinetics can be slowed appreciably in densely packed monolayers or in monolayers where the redox center is buried.[50−54] The decrease in electron-transfer rates observed here for all the monolayers as the surface concentration increases (Figure 7) has also been reported for a number of other porphyrin monolayers.[7,27,31] This mechanism would suggest that the rates for a given class of monolayers with the different Group VI anchoring atoms might diverge at very low surface coverage. This is not apparent from the data; however, the rates are difficult to measure accurately at very low surface coverage due to the low amount of current.

The above comments notwithstanding, we do not have a completely satisfactory explanation for the detailed nature of the electron-transfer characteristics of the different types monolayers. Indeed, the rates may be influenced by a complex interplay of factors that vary as a function of both linker type and surface coverage. This view is supported by the general trends observed for the plots of k_0 versus Γ for the molecules bearing the $-\mathbf{Bz}-$ versus $-\mathbf{CH_2}-$ class of linkers (Figure 7). In particular, while the rate versus coverage plots for the $-\mathbf{CH_2}-$ class appear to indicate a single process with log-linear behavior, those for the $-\mathbf{Bz}-$ monolayers appear to be characterized by two competing processes instead (note the sharp break observed at intermediate coverages).

V. Conclusions

The studies reported herein demonstrate that porphyrin monolayers on Si(100) can be readily prepared with different

(47) Roth, K. M.; Liu, Z.; Gryko, D. T.; Clausen, C.; Lindsey, J. S.; Bocian, D. F.; Kuhr, W. G. *ACS Symp. Series* **2003**, *844*, 51−61.
(48) Roth, K. M.; Lindsey, J. S.; Bocian, D. F.; Kuhr, W. G. *Langmuir* **2002**, *18*, 4030−4040.
(49) Smalley, J. F.; Finklea, H. O.; Chidsey, C. E. D.; Linford, M. R.; Creager, S. E.; Ferraris, J. P.; Chalfant, K.; Zawodzinsk, T.; Feldberg, S. W.; Newton, M. D. *J. Am. Chem. Soc.* **2003**, *125*, 2004−2013.
(50) Creager, S.; Yu, C. J.; Bamdad, C.; O'Connor, S.; MacLean, T.; Lam, E.; Chong, Y.; Olsen, G. T.; Luo, J.; Gozin, M.; Kayyem, J. F. *J. Am. Chem. Soc.* **1999**, *121*, 1059−1064.
(51) Sachs, S. B.; Dudek, S. P.; Hsung, R. P.; Sita, L. R.; Smalley, J. F.; Newton, M. D.; Feldberg, S. W.; Chidsey, C. E. D. *J. Am. Chem. Soc.* **1997**, *119*, 10563−10564.
(52) Sikes, H. D.; Smalley, J. F.; Dudek, S. P.; Cook, A. R.; Newton, M. D.; Chidsey, C. E. D.; Feldberg, S. W. *Science* **2001**, *291*, 1519−1523.
(53) Sumner, J. J.; Creager, S. E. *J. Phys. Chem. B* **2001**, *105*, 8739−8745.
(54) Campbell, D. J.; Herr, B. R.; Hulteen, J. C.; Van Duyne, R. P.; Mirkin, C. A. *J. Am. Chem. Soc.* **1996**, *118*, 10211−10219.
(55) Paynter, R. W. *Surf. Interface Anal.* **1981**, *3*, 186−187.

linker groups and anchoring atoms. This permits the characterization of the structural and electron-transfer properties of the different resulting types of monolayers, and opens the possibility of exploring a wide variety of other redox-active molecular architectures on semiconductor platforms. On the other hand, the electronic properties of the monolayers depend in a complex manner on a number of physical properties such as bonding motif, adsorption geometry, and molecular surface packing, thereby limiting the ability to predict the electronic properties from first principles. A complete understanding of the interrelation of these factors will require additional systematic studies on a broader class of porphyrinic molecules bearing different types of redox-active units and linker architectures.

Acknowledgment. This work was supported by the Center for Nanoscience Innovation in Defense and DARPA/DMEA (under award number H94003-04-2-0404) and by ZettaCore, Inc. We thank J. Diers for obtaining the solution electrochemical data.

Supporting Information Available: Complete synthetic procedures and spectral data for *tol*-**ZnPCH$_2$OH**. This material is available free of charge via the Internet at http://pubs.acs.org.

JA045243W